Ultrafast Tracking of Oxygen Dynamics during Proton FLASH

SUPPORTING INFORMATION

Mirna El Khatib, PhD,[a]* Alexander L. Van Slyke, PhD,[b]* Anastasia Velalopoulou, PhD,[b] Michele M. Kim, PhD,[b] Khayrullo Shoniyozov, PhD;[b] Srinivasa Rao Allu, PhD,[a] Eric E. Diffenderfer, PhD,[b] Theresa M. Busch, PhD,[b] Rodney D. Wiersma, PhD,[b] Cameron J. Koch, PhD,[b] Sergei A. Vinogradov, PhD[a]

* Equal contributions.

Affiliations

[a] *Department of Biochemistry and Biophysics, Perelman School of Medicine, and Department of Chemistry, School of Arts and Sciences, University of Pennsylvania, Philadelphia, PA 19104*

[b] *Department of Radiation Oncology, Perelman School of Medicine, University of Pennsylvania, Philadelphia, PA 19104*

Corresponding authors

Sergei A. Vinogradov, PhD; E-mail: vinograd.upenn@gmail.com

Cameron J. Koch, PhD; E-mail: kochc@pennmedicine.upenn.edu

Table of Contents

1. Image of the experimental setup used in irradiation experiments

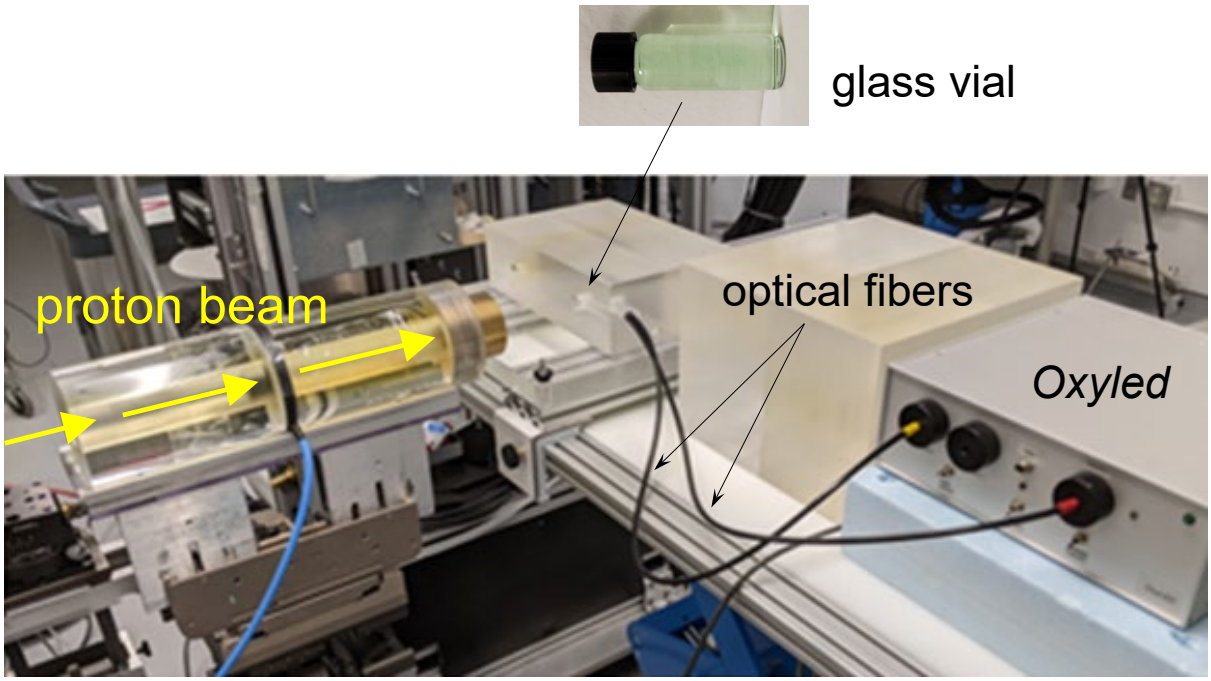

Glass vial (4 ml) filled with a solution containing PtG4, sealed and positioned in the path of a collimated proton beam.

2. Brief description of *Oxyled* phosphorometer

The instrument is constructed around a 16-bit multichannel data acquisition board (USB NI-6341, National Instruments) with AD/DA converter operating at 500 kHz frequency. The board communicates with a host computer *via* the USB bus. The excitation sources in the instrument are light-emitting diodes (Ledengin, LZ1, 630 nm), having the rise time ~50 ns. Alternatively, the instrument can operate with a modulated laser diode (Power Technology, IRF 50 ns) as an excitation source, which allows focusing the excitation light into a spot ~100 μm in diameter. The detector in the instrument is an avalanche photodiode module (APD C12703-01, Hamamatsu), response time 3.3 μs.

The excitation light is carried to the sample by a plastic fiber (4 mm in diameter), and the phosphorescence is collected by another similar fiber, whose tip is positioned immediately next to the tip of the excitation fiber. The phosphorescence is passed through a long-pass filter (730 nm, Asahi Spectra), focused on the aperture of the APD, and the APD current is digitized.

3. Spike removal algorithm

The spikes occurring in the phosphorescence decays due to interfering radiation (protons) cannot be treated as random noise, and hence conventional methods for data smoothing (running average, median filters etc) are not applicable. Hence, a specialized algorithm for detection of spikes and their removal is required.

In brief, a pointer is moved along the array of numbers, which represent the phosphorescence decay, and a difference between the current and the previous number is calculated. If this difference is larger than a pre-set threshold value, a flag is raised. If the next encountered difference is again larger than the threshold, a spike is considered detected. The pointer continues along the array until the end of the spike is found, i.e. the current value is below the pre-spike value. In some cases additional analysis is necessary, because spikes can be followed by a few oscillations.

After all the points comprising a spike are defined, they are taken out of the data array, and the same is done for all subsequent spikes. The resulting decay has "holes" in it instead of spikes. These holes, however, have no effect on fitting, except that a decay with holes has fewer data points. Furthermore, because spikes appear randomly along the decay, averaging several decays with holes generates a decay essentially with no holes.

The algorithm was extensively tested using synthetic data with added noise and spikes of different magnitude. These simulations confirmed that removing spikes does not introduce any systematic error in the computed (by fitting) decay rates/lifetimes, as expected.

4. Quenching of phosphorescence of Oxyphor PtG4 by H_2O_2

For determination of the effect of H_2O_2 on the phosphorescence of PtG4, aliquots of aqueous H_2O_2 were added to a solution of PtG4, either in distilled water or in water containing BSA (2%), and the phosphorescence lifetime was determined. The system for phosphorescence/oxygen titrations has been described previously.[1, 2] A solution of Oxyphor PtG4 (10 mL, 1 μM) in distilled water was kept inside a dark thermostatic chamber at equilibrium with air at 23°C under gentle stirring. The phosphorescence decay times were measured with 0.5 Hz frequency. Aliquots of a stabilized 100 mM solution of H_2O_2 (Sigma-Aldrich) were added in portions to the solution such that each addition corresponded to an increase in [H_2O_2] by ~500 μM, which approximately matches the amount of H_2O_2 produced if all oxygen in an aqueous solution equilibrated with air (~250 μM [O_2]) would be radiolytically converted into H_2O_2, the final thermodynamically stable product (according to the reaction $2H_2O+O_2+\text{radiation}\rightarrow 2H_2O_2$, which implicitly contains the reduction of O_2 to superoxide and its subsequent disproportionation).

Two types of experiments were performed: when the solution was equilibrated with air and when the solution was fully deoxygenated by argon. Both titrations produced similar results, however measurements in deoxygenated solutions are less reliable, and, as expected, gave slightly lower quenching efficiency for H_2O_2. When an aliquot of a stock solution of H_2O_2 is added to a deoxygenated (by argon flow) solution of the probe, some oxygen is inevitably introduced into that solution as well. To remove these small traces of oxygen, the solution needs to be kept under argon and stirring for additional time (typically many minutes) until the phosphorescence lifetime stops changing. During that time, H_2O_2 gradually decomposes, since the stabilizer, which was present in the stock solution at a high concentration, is diluted upon injection of the stock into the measurement solution as well. As a result, the effective quantity of H_2O_2 present in the solution by the time when it is fully deoxygenated is less than injected.

A phosphorescence lifetime trace recorded in a typical experiment performed on air is shown in Fig. S1.

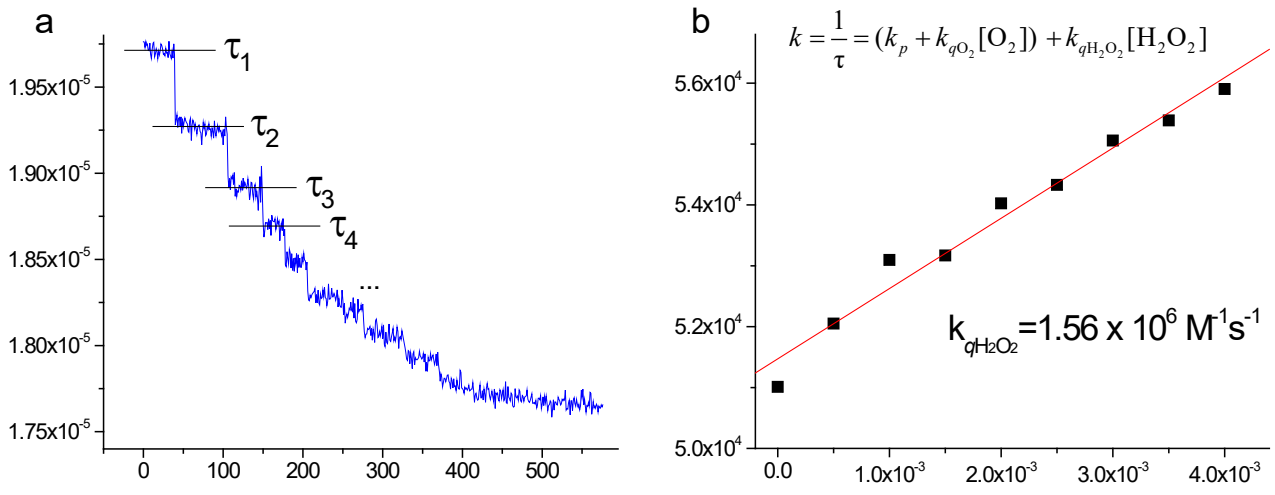

Figure S1. (a) Phosphorescence lifetime trace during additions of H_2O_2 (in 500 μM steps) to a solution of PtG_4 in water. (b) The corresponding Stern-Volmer plot for quenching of phosphorescence of PtG4 by H_2O_2.

After each addition, a series of data points were averaged, giving a sequence of lifetimes τ_1, τ_2, τ_3... (Fig. S1a), which were used to construct a Stern-Volmer plot (Fig. 1b). The obtained quenching constant k_{qH2O2} was found to be ~1.56×10^6 $M^{-1}s^{-1}$, which is ~80 times less than the quenching constant for oxygen, k_{qO2}~1.26×10^8 $M^{-1}s^{-1}$. An even lower constant was obtained in solutions containing BSA.

5. Oxygen depletion baseline

To verify that the slopes of the baselines in the oxygen depletion traces, seen in some experiments, were not caused by photochemical depletion of oxygen, a vial (4 mL) containing a solution of BSA (5%) in phosphate buffer (20 mM, pH 7.2) was tightly sealed, leaving no air bubbles under the cap, and the phosphorescence lifetime trace was recorded using the excitation light exposures identical to what was used in the oxygen depletion experiments involving radiation. In another experiment, 100 times less light was used for excitation, and a similar trace was recorded. The results are shown in Fig. S2, confirming that the baseline slope was not caused by the photochemical depletion of oxygen. The slopes were likely caused by the respiration of bacteria that were introduced into the solutions with albumin. These solutions could not be purified by filtration through antibacterial filters due to their viscosity. Importantly, these slopes were small and had no effect on the oxygen depletion measurements.

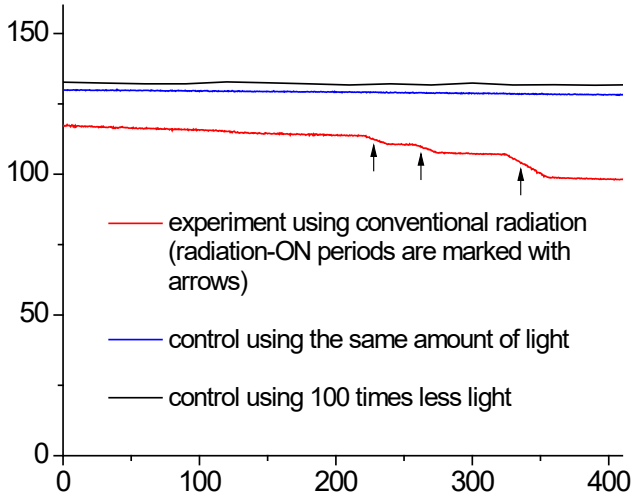

Figure S2. Phosphorescence lifetime traces verifying that the baseline slopes were not caused by photochemical depletion of oxygen.

6. Modeling oxygen consumption in solution subjected to radiation

The system was modeled as a homogeneous solution of a hypothetical organic molecule RH in water. The simulations consisted of numerical integration of a system of differential equations describing the evolution of the system's components. The code was written in C/C++ (Qt, Nokia). The reactions shown in Scheme 1 were considered, whereby the processes occurring with relatively high fluxes (under the conditions of our experiments, i.e. ~millimolar concentration of organic substrate) are shown in blue and processes occurring at very small fluxes - in grey. Reactions (12), (16) and (17) are commented on in the Table below.

Scheme 1

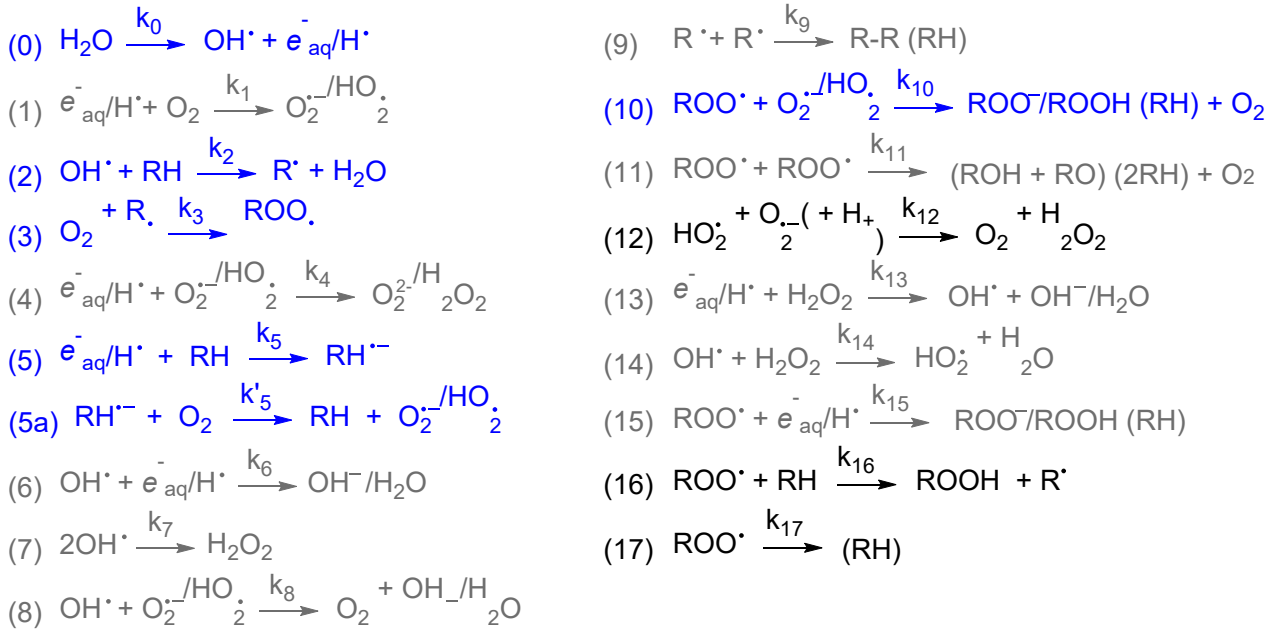

Several simplifications were used:

1) Radiation was treated as a homogeneous field acting uniformly on the entire solution volume. This kind of treatment cannot reproduce reactions along particle tracks (e.g. radical recombinations), which require direct Monte-Carlo-based methods,[3] it can be instrumental in evaluation of individual effects of different processes composing the complex system.[4]

2) Direct ionization of the organic substrate (RH) was ignored in view of the fact that its radiolytic yield in water is significantly lower than that of water itself at the concentrations used in our experiments, and the subsequent oxidation/reduction of RH by the primary products of water radiolysis is extremely efficient.

3) Each conjugated Brønsted acid/base pair (e.g. e^-_{aq}/H$^\bullet$, $O_2^{\bullet-}$/$HO_2^\bullet$) was treated as a single species. While we recognize that the rate constants of the reactions involving these species individually are different, in most cases the differences are no more than by an order of magnitude, and, more importantly, there are many other approximations/unknowns in the model that can have a profound effect on the outcome, and for the purpose of this initial estimation, this simplification was deemed reasonable. The corresponding rate constants used in the calculations were set simply as averages of the corresponding individual values. Obviously, a more accurate treatment would involve acid/base equilibria, e.g. as described in ref. [4].

4) Since the substrate in our experimental system was a large protein (BSA, MW ~65 kDa), and each oxidation introduced just a single peroxo- or oxo- or hydroxyl group into its structure (converting it to ROOH, RO or ROH, respectively), the rest of the molecule remained unchanged and was available for subsequent oxidations. Therefore, it was effectively returned to the substrate pool, which is shown in the scheme above by the symbol (RH) after the respective reaction products.

5) The reduction of the substrate by free electrons or hydrogen atoms (reaction (5)), followed by reduction of oxygen (reaction (5a)) is expected to be strongly substrate-dependent, and in the case of BSA it would probably involve mostly the reduction/oxidation of the disulfide bridges -S-S-.

6) The reactions involving peroxyl radicals (ROO$^\bullet$) may involve chain initiation, propagation, and termination steps (3, 16, 17 and 10). Typically these reactions are discussed in the context of lipid peroxidation, but other organic molecules potentially can be subject to these transformations as well. The rates of these processes are difficult to predict, as they would depend significantly on the substrate. It is the balance between the rate constants of these steps that defines, to a large degree, the total oxygen depletion *g*-values. In order to gain control over the rate of these processes we considered a hypothetical monomolecular chain termination step (reaction (17)) which allowed us to smoothly adjust the rate of oxygen consumption, bringing it closer to the experimentally observed level. In principle, the same control could be achieved by carefully balancing the rate constants for these reactions, but using a single rate constant (k_{17}) was just simpler. Importantly, using different chain propagation and initiation rate constants had minimal effect on the profile of the *g*-value dependence in the low [O_2] region, which was the main focus of our simulations.

Considering these approximations, the total number of components in the system was 10 (H_2O, e^-_{aq}/H$^\bullet$, OH$^\bullet$, RH, RH$^{-\bullet}$, R$^\bullet$, O_2, $HO_2^\bullet$, H_2O_2, ROO$^\bullet$) and the number of reactions was 19. The values of the rate constants for the reactions in Scheme 1 are shown in Table 1. The constants were taken from refs. [4, 5], unless noted separately. An example of a rate equation (for OH$^\bullet$) is shown below:

$$\frac{d[\mathrm{OH}^\bullet]}{dt} = k_0[\mathrm{H_2O}] + k_{13}[e^-_{aq}][\mathrm{H_2O_2}] - k_2[\mathrm{OH}^\bullet][\mathrm{RH}] - k_6[\mathrm{OH}^\bullet][e^-_{aq}] - k_7[\mathrm{OH}^\bullet][\mathrm{OH}^\bullet] - k_8[\mathrm{OH}^\bullet][\mathrm{HO_2}^\bullet] - k_{14}[\mathrm{OH}^\bullet][\mathrm{H_2O_2}]$$

Integration was performed using the piece-wise linear approximation method. The entire simulation run was divided into periods of radiation-ON and radiation-OFF, mimicking our experimental conditions. The time grid steps for the ON and OFF periods were 10^{-8} s and 10^{-5}s, respectively. The optimal steps sizes were validated by performing simulations using 10 and 100 times finer grids, which confirmed that reducing the grid step did not introduce changes to the solution.

For the simulations mimicking our experiments (oxygen depletion in closed vials) the starting concentrations of all components were to set to zero, except for O_2 (typically, $[O_2]_0$=275 μM) and RH ($[RH]_0$=0.8 mM). The latter value was calculated based on the molecular weight of BSA (~64 kDa) for 5% (by weight) solution. During the radiation-ON periods, constant k_0 was set to the value calculated as shown in Table 1. During radiation-OFF periods, it was set to zero. The duration of each radiation-ON period was set by the total dose that had to be deposited on the sample. For example, to deposit a dose of 10 Gy at the rate of 100 Gy/s, the radiation-ON period was 100 ms, and the simulated trace for each component consisted of 10^7 data points. The radiation-OFF periods typically were 4 s-long. The simulation continued until a pre-selected low-threshold oxygen concentration was reached (e.g. $[O_2]=10^{-9}$ M). The code also allowed us to perform simulations in open systems, mimicking *in vivo* runs, where only one dose was deposited starting with any arbitrary $[O_2]$ and all other components' concentrations (except [RH]) were zero.

Table 1. Rate constants used in simulations.

Rate const.	**Value ($M^{-1}s^{-1}$)**	**Notes**
k_0 [a]	$g_{H_2O}\times R/[H_2O]$ [b]	-
k_1	1.9×10^{10}	-
k_2	1.0×10^{10}	-
k_3	1.0×10^{6} - 1.0×10^{10}	the value of k_3 was varied in order to mimic the experimental *g*-value oxygen dependence
k_4	1.3×10^{10}	-
k_5	1.0×10^{8}	this value was chosen arbitrarily; the literature values for similar constants for small molecules are in the range of 10^9 $M^{-1}s^{-1}$; by analogy with other constants whose values are reduced by ~10-fold citing the large size of the substrate, k_5 was adjusted accordingly; however, we note that raising this

		constant up to 10^{10} $M^{-1}s^{-1}$ did not result in strong changes in the profile of the oxygen dependence.
k'_5	1.0×10^8	the same rationale as above
k_6	3.0×10^{10}	-
k_7	5.5×10^9	-
k_8	8.0×10^9	-
k_9	1.0×10^6	the value of this constant could be much lower due to the large size of the BSA radicals
k_{10}	1.0×10^4	similar to k_5, the value of this constant was reduced by 10-fold compared to the constants published for some small molecules; this reaction (10) is likely to be the main step leading to the complete consumption of superoxide under our experimental conditions.
k_{11}	1.0×10^4	the value of this constants could be much lower due to the large size of the BSA radicals
k_{12}	1.0×10^4	disproportionation of superoxide/hydroperoxyl radicals at pH~7 occurs primarily *via* the pathway shown in (12); however, for more accurate description of disproportionation all pathways need to be considered;[6] in any case, in the absence of catalysts (superoxide dismutase) the flux through the dismutation pathway is likely to be quite low; on the other hand, BSA samples may contain traces of Fe^{3+} and maybe even traces of superoxide dismutase.
k_{13}	1.1×10^{10}	-
k_{14}	2.7×10^7	-
k_{15}	1.0×10^9	as in the case of k_5 and k_{10}, the value was reduced by 10-fold compared to the values published for small molecules.
k_{16}	5.0×10^7	the rate of the chain propagation step and the chain termination step (k_{17}) were balanced to keep the *g*-values similar to those experimentally obtained.
k_{17} [a]	5.0×10^5	see above

[a] Units: s^{-1}.

[b] g_{H_2O} - *g*-value for water radiolysis: 0.27×10^{-6} M/Gy; R - dose rate (Gy/s) $[H_2O]$=55.55 M.

References

1. Rozhkov V, Wilson D, Vinogradov S. Phosphorescent Pd porphyrin-dendrimers: Tuning core accessibility by varying the hydrophobicity of the dendritic matrix. *Macromolecules* **35**, 1991-1993 (2002).

2. Khajehpour M, Rietveld I, Vinogradov S, Prabhu NV, Sharp KA, Vanderkooi JM. Accessibility of Oxygen with Respect to the Heme Pocket in Horseradish Peroxidase. *Proteins-Struct Func Gen* **53**, 656-666 (2003).

3. Boscolo D, Scifoni E, Durante M, Krämer M, Fuss MC. May Oxygen Depletion Explain the FLASH Effect? A Chemical Track Structure Analysis. *Radiother Oncol* **162**, 68-75 (2021).

4. Labarbe R, Hotoiu L, Barbier J, Favaudon V. A Physicochemical Model of Reaction Kinetics Supports Peroxyl Radical Recombination as the Main Determinant of the FLASH Effect. *Radiother Oncol* **153**, 303-310 (2020).

5. Buxton GV, Greenstock CL, Helman WP, Ross AB. Critical Review of Rate Constants for Reactions of Hydrated Electrons, Hydrogen Atoms and Hydroxyl Radicals in Aqueous Solution. *J Phys Chem Ref Data* **17**, 513-886 (1988).

6. Bielski BHJ, Allen AO. Mechanism of Disproportionation of Superoxide Radicals. *J Phys Chem* **81**, 1048-1050 (1977).